Geoscience Letters

RESEARCH LETTER

Open Access

Absence of Cretaceous hairpin in the apparent polar wander path of southwest Japan: consistency in paleomagnetic pole positions

Koji Uno[1,2*], Honoka Ohara[2], Kuniyuki Furukawa[3] and Tatsuo Kanamaru[4]

Abstract

To test the hypothesis that a Cretaceous hairpin turn is absent in the apparent polar wander path (APWP) of the inner arc of southwestern Japanese island (southwest Japan), we refined a mid-Cretaceous (100 Ma) paleomagnetic pole from southwest Japan. Red mudstone samples from the 100 Ma Hayama Formation were collected for paleomagnetic analysis from eight sites in the Hayama area in the central part of southwest Japan. A high-temperature remanent magnetization component carried by hematite was isolated from these sites and was found to be of primary mid-Cretaceous origin. The primary nature of the magnetization is supported by the detrital character of the magnetic carrier. The primary directions provided a paleomagnetic pole (35.0°N, 209.6°E, $A_{95} = 6.1°$, $N = 8$), which represented southwest Japan at 100 Ma. This pole falls into a cluster of Cretaceous poles in southwest Japan. An APWP for southwest Japan between 110 and 70 Ma was updated to ascertain the stationarity of the pole positions for this region. Therefore, it is unlikely that the APWP for southwest Japan experienced a hairpin turn during the Cretaceous.

Keywords Apparent polar wander path, Hairpin turn, Cretaceous, Southwest Japan

Introduction

A series of paleomagnetic poles across geological time-periods from a continent, cratonic block, or continental fragment forms an apparent polar wander path (APWP). APWPs from geological domains have been used to assess the speed of drift in a domain and the collision process between domains.

A hairpin turn (also called a cusp) on an APWP reflects an abrupt change in continental motion (Gordon et al. 1984). During the early construction stage of the APWP for a region, the age and position of the hairpins would change significantly due to lack of data. Westphal et al. (1986) built an APWP for Eurasia and identified a remarkable hairpin around the mid-Cretaceous period. This hairpin in the APWP was revised according to Besse and Courtillot (1991), where the Cretaceous hairpin was moved to an older age of approximately 120 Ma. These authors made further improvements to the APWP, moving the Cretaceous hairpin to an even older age (~ 140 Ma) and an additional one in the Jurassic (Besse and Courtillot 2002).

A hairpin was observed in an APWP for the inner arc of the southwestern Japanese islands (henceforth referred to as southwest Japan). This region constituted the easternmost part of East Asia during the Mesozoic (Otofuji

*Correspondence:
Koji Uno
kojiuno@shse.u-hyogo.ac.jp
[1] Laboratory of Geosciences, School of Human Science and Environment, University of Hyogo, 1-1-12 Shinzaike-honcho, Himeji 670-0092, Japan
[2] Department of Earth Sciences, Okayama University, 3-1-1 Tsushimanaka, Kita-ku, Okayama 700-8530, Japan
[3] Faculty of Business Administration, Aichi University, 4-60-6 Hiraike-cho, Nakamura-ku, Nagoya 453-8777, Japan
[4] Department of Earth and Environmental Sciences, Nihon University, 3-25-40 Sakurajosui, Setagaya-ku, Tokyo 156-8550, Japan

et al. 1985; Jolivet et al. 1994; Lee 2008) (Fig. 1a), and its APWPs have been proposed from the Early Cretaceous onward (Otofuji and Matsuda 1987; Kodama and Takeda 2002; Uno et al. 2017, 2021). The mid-Cretaceous (100 Ma) paleomagnetic pole for southwest Japan is located at a near-sided position with respect to those of the previous (110 Ma) and subsequent (90–70 Ma) ages (Fig. 1b). As the 110–70 Ma poles for East Asia show no significant polar motion (Cogné et al. 2013), southwest Japan is postulated to have experienced northward tectonic translation as far as 2000 km between 110 and 100 Ma with respect to East Asia, followed by a southward translation of the same magnitude of this region between 100 and 90–70 Ma (Kodama and Takeda 2002). However, this successive tectonic movement is unlikely within the tectonic setting of the East Asian margins, including the relevant oceanic plate motion (Uno et al. 2017).

This observation may be relevant to the tectonic scenario in southwest Japan. When a hairpin shape in an APWP depends on a single pole, that is, when only one pole appears to detour, the hairpin may easily disappear or move significantly in time and position by subsequent improvement of the pole position. For example, Seguin and Zhai (1992), one of the pioneering works in the construction of APWP for the South China Block, found two hairpins in the APWP during the Late Permian (251 Ma) and Late Triassic (222 Ma). Each hairpin was characterized by a single paleomagnetic pole. Huang et al. (2018) refined the APWP for the South China Block, in which the former hairpin was moved to an older age of the Early Permian (290 Ma) and the latter was moved to the Middle Triassic (240 Ma). Therefore, further studies in southwest Japan may elucidate whether the hairpin in the APWP for this region is an essential element around the mid-Cretaceous.

The mid-Cretaceous (100 Ma) Hayama Formation in the Hayama area (34.82°N, 133.49°E) in the central part of southwest Japan (H in Fig. 1a) was selected as our study site. This area is the most suitable for determining the Mesozoic paleomagnetic pole, which is representative of southwest Japan, as Sonehara et al. (2020) demonstrated that the land on which the Hayama Formation was deposited was the most stable continental tectonic unit in southwest Japan. At present, it is detached from East Asia due to the formation of the Japan Sea in the

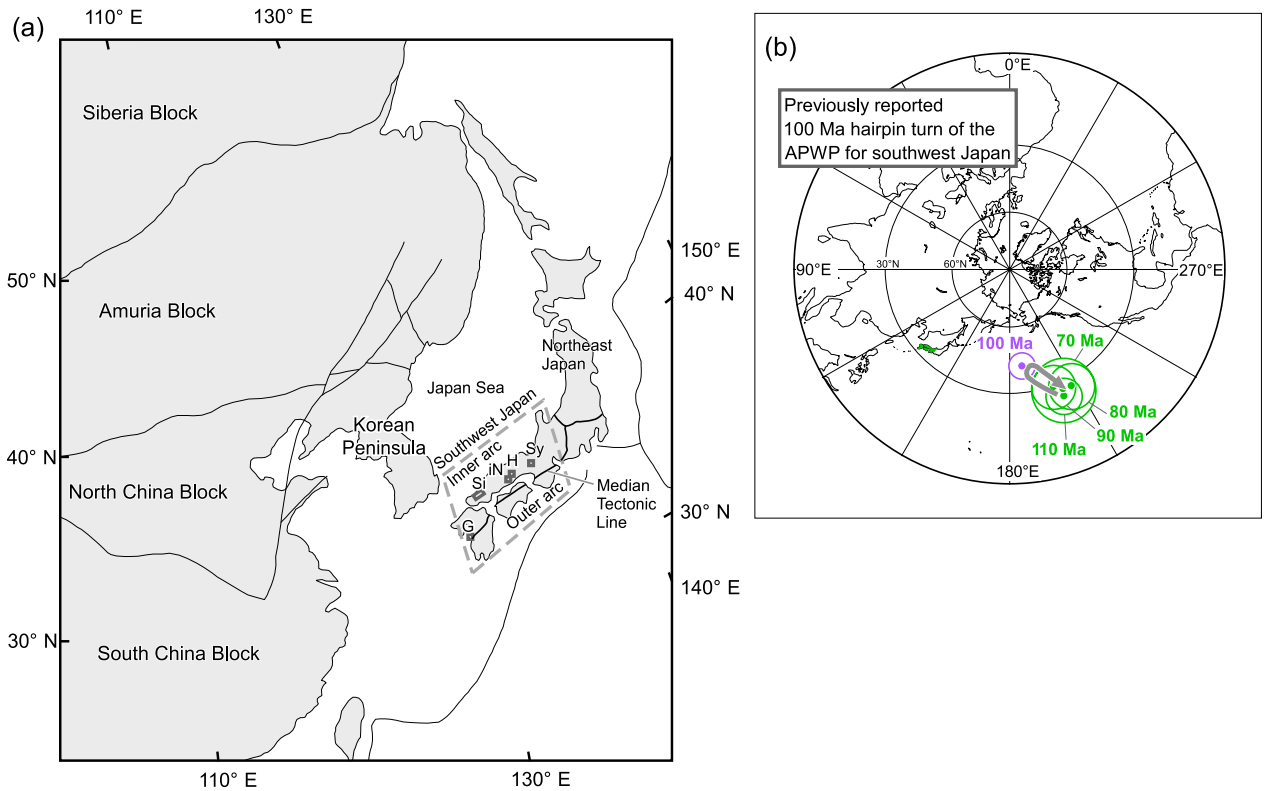

Fig. 1 **a** Tectonic outline map of East Asia and the Japan Arc. *G* Goshonoura area, *Si* San'in area, *iN* Inakura area, *H* Hayama area (study area), *Sy* Sasayama area. The Median Tectonic Line demarcates southwest Japan into the inner and outer arcs. **b** Previously proposed APWP for southwest Japan, except the 100 Ma pole (Uno et al. 2021). The 100 Ma pole (187.8°N and 40.6°E with $A_{95} = 5.7°$) is a site-based mean pole calculated in this study using data from Otofuji and Matsuda (1987) and Kodama and Takeda (2002)

Cenozoic. This letter presents a paleomagnetic pole from the 100 Ma Hayama Formation to replace and interpolate the Cretaceous APWP for southwest Japan and suggests an absence of the Cretaceous hairpin for this region.

Geological setting and sampling

The mid-Cretaceous Hayama Formation is exposed in central southwest Japan (Fig. 1a). It is a fluvial deposit formed by filling of the river valleys. The Hayama Formation, with a total stratigraphic thickness of approximately 300 m, is divided into three parts: Limestone conglomerate, Eda conglomerate, and Sora mudstone members, from the oldest to youngest (Suzuki et al. 2001). The Limestone conglomerate was derived from basement limestones of the Carboniferous-Permian age. The Eda conglomerate member is mainly composed of clast-supported layers consisting of subrounded gravels. The Sora mudstone member is composed of red mudstones and intercalates a rhyolitic tuff layer that yielded a zircon fission track age of 101 ± 4 Ma (Suzuki et al. 2001). No faults affect the distribution of the Hayama Formation. The geological structure of the Hayama Formation has a largely flat attitude, and no folding is inferred to have occurred in this area (Suzuki et al. 2001). The Hayama Formation is overlain by the Paleogene Kibi Group that has zircon fission track aged 35.8–27.1 Ma and shows no significant tilting (Suzuki et al. 2003).

Samples of red mudstones from the Sora mudstone member (sites HY1–HY8) of the Hayama Formation were collected from eight sites for paleomagnetic analysis (Fig. 2). The sampling sites were distributed over an area of ~ 4 × 1.5 km. Each site contained 7–9 samples. Bedding at the sampling sites was flat or gentle (flat to 6°). All samples were collected by hand and oriented in the field using a magnetic compass attached to a tripod. Present-day geomagnetic field declinations at sampling sites were determined using the International Geomagnetic Reference Field (IGRF) model.

Paleomagnetism and rock magnetism

The initial natural remanent magnetization (NRM) intensity of the red mudstone samples ranged between 3.2×10^{-2} and 8.1×10^{-2} A m^{-1} (mean of 4.8×10^{-2} A m^{-1}). A low-temperature component (LTC) was identified in samples from all eight sites. It showed normal polarity and was removed in the initial stages of demagnetization at ~ 200 °C. After removal, a medium-temperature component (MTC) was observed at all the sites. This component is of normal polarity and shows a large decay in intensity until its unblocking temperature (~ 650 °C). Following the removal of the component, a high-temperature component (HTC) that decayed to the origin was identified at all the sites and showed normal polarity. HTC was eventually unblocked at 695 °C (Fig. 3).

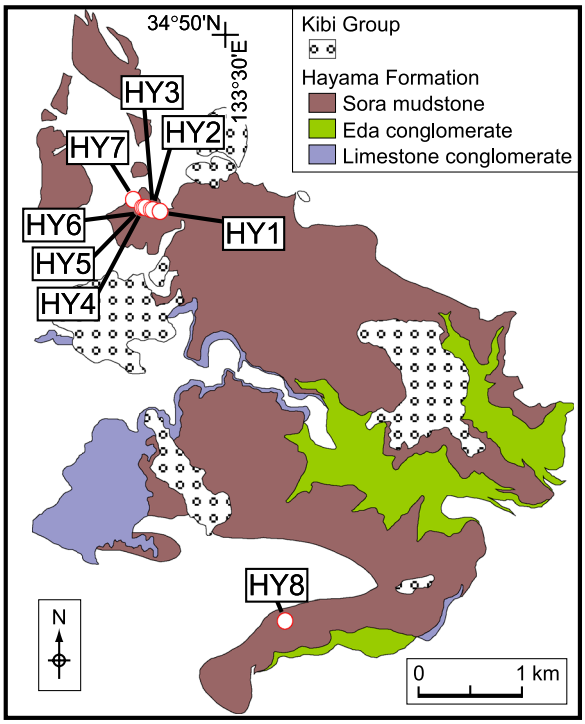

Fig. 2 Geological map of the Hayama Formation in the Hayama area (Suzuki et al. 2001). Open circles denote the paleomagnetic sampling sites

The results of thermal demagnetization of the three-component isothermal remanent magnetization (IRM) showed that the remanent magnetization predominantly resides in hematite. The high-coercivity (2.5 T) magnetization was dominant and showed a relatively gradual decay up to 620–650 °C, after which the magnetization abruptly decayed and was completely unblocked by 695 °C (Fig. 4a). Another magnetic phase with an unblocking temperature of ~ 580 °C was observed in the low-coercivity (120 mT) component, suggesting the presence of a certain amount of magnetite.

The directions of LTC before tilt correction roughly conform to the present Earth's field direction ($D = 352.1°$, $I = 49.6°$) and geocentric axial dipole field direction ($D = 0°$, $I = 54.3°$) in the study area (Fig. 5a, Table 1). Considering its unblocking temperatures, this component can be attributed to viscous remanent magnetization. MTC was found to pass through 580 °C, the Curie temperature of magnetite, during thermal demagnetization. Because MTC may be partly carried by magnetite (the presence of which was identified by the IRM experiment) and partly by hematite, we separated the components before and after 580 °C; we will refer to them as MTC1

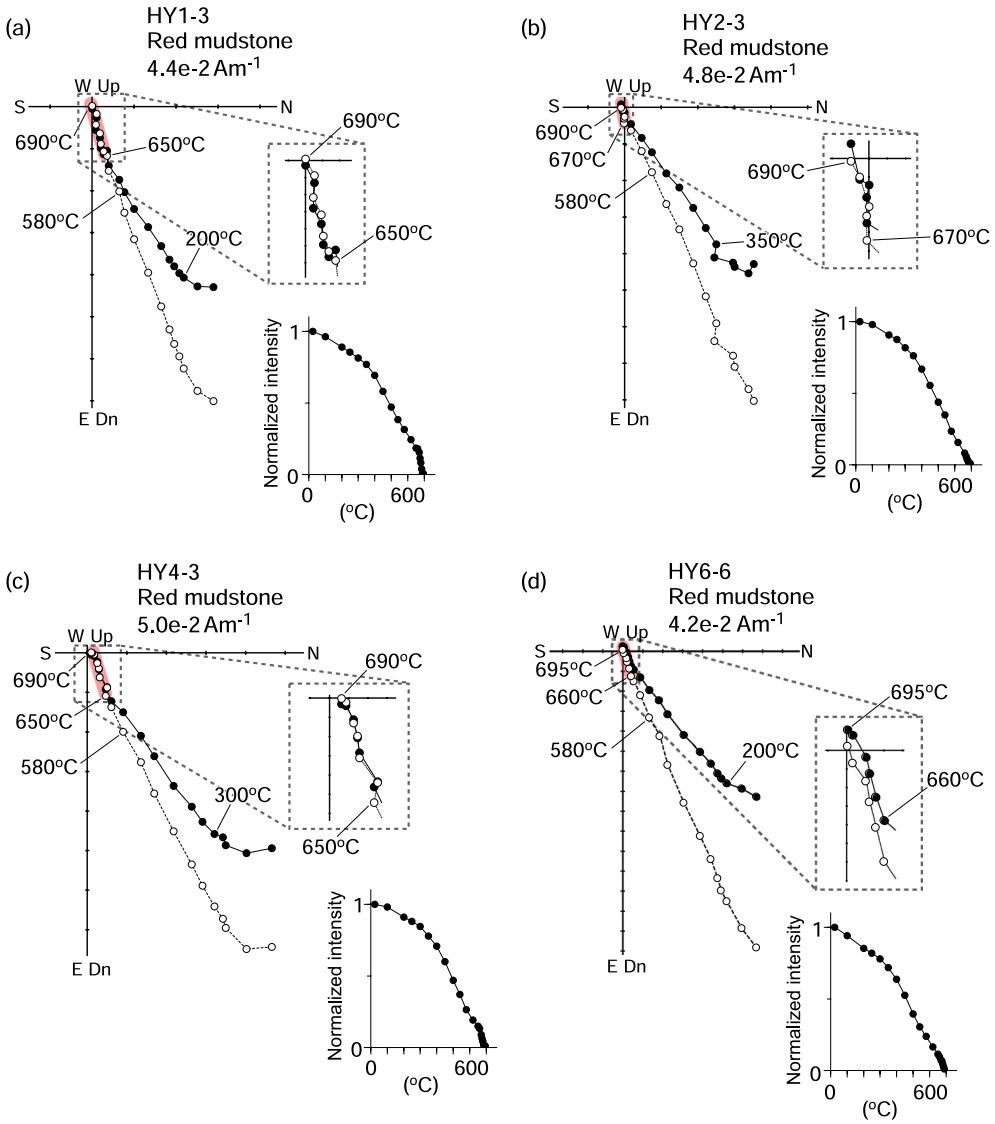

Fig. 3 Representative orthogonal plots and normalized remanence intensity curves of thermal demagnetization results of red mudstones in geographic coordinates. Solid and open symbols on orthogonal plots represent projections on the horizontal and vertical planes, respectively. The highlighted magnetization component denotes the high-temperature remanent magnetization component

and MTC2 according to the order of appearance during thermal demagnetization. The directions of MTC1 and MTC2 before and after the tilt correction are shown in Fig. 5a. The directions of both components are close to each other, with little change in direction before and after the tilt correction. McFadden's (1990) fold test yielded an inconclusive test result at the 95% confidence level for both components. The directions of MTC1 and MTC2 before tilt correction were compared with those of the previously observed medium-temperature component of Cretaceous red beds from southwest Japan (Inakura and Sasayama areas, iN and Sy in Fig. 1a): $D = 51.6°$ and $I = 54.3°$, with $\alpha_{95} = 4.8°$ ($N = 20$), calculated using directions of the Inakura Formation at 12 sites (Uno et al. 2021) and the Sasayama Group at 8 sites (Uno and Furukawa 2005). The directions of MTC1 and MTC2 were similar to those reported previously (Fig. 5b), suggesting secondary magnetization. We next compared these directions to the reference direction for southwest Japan at 70 and 20 Ma (Uno et al. 2021). The directions of MTCs differed from the 70 Ma reference direction, indicating that the age of these directions postdates 70 Ma. The directions, in contrast, were similar to the 20 Ma reference direction. Furthermore, we observed that the directions of each MTC slightly improved clustering after tilt correction (Table 1). Therefore, we speculate

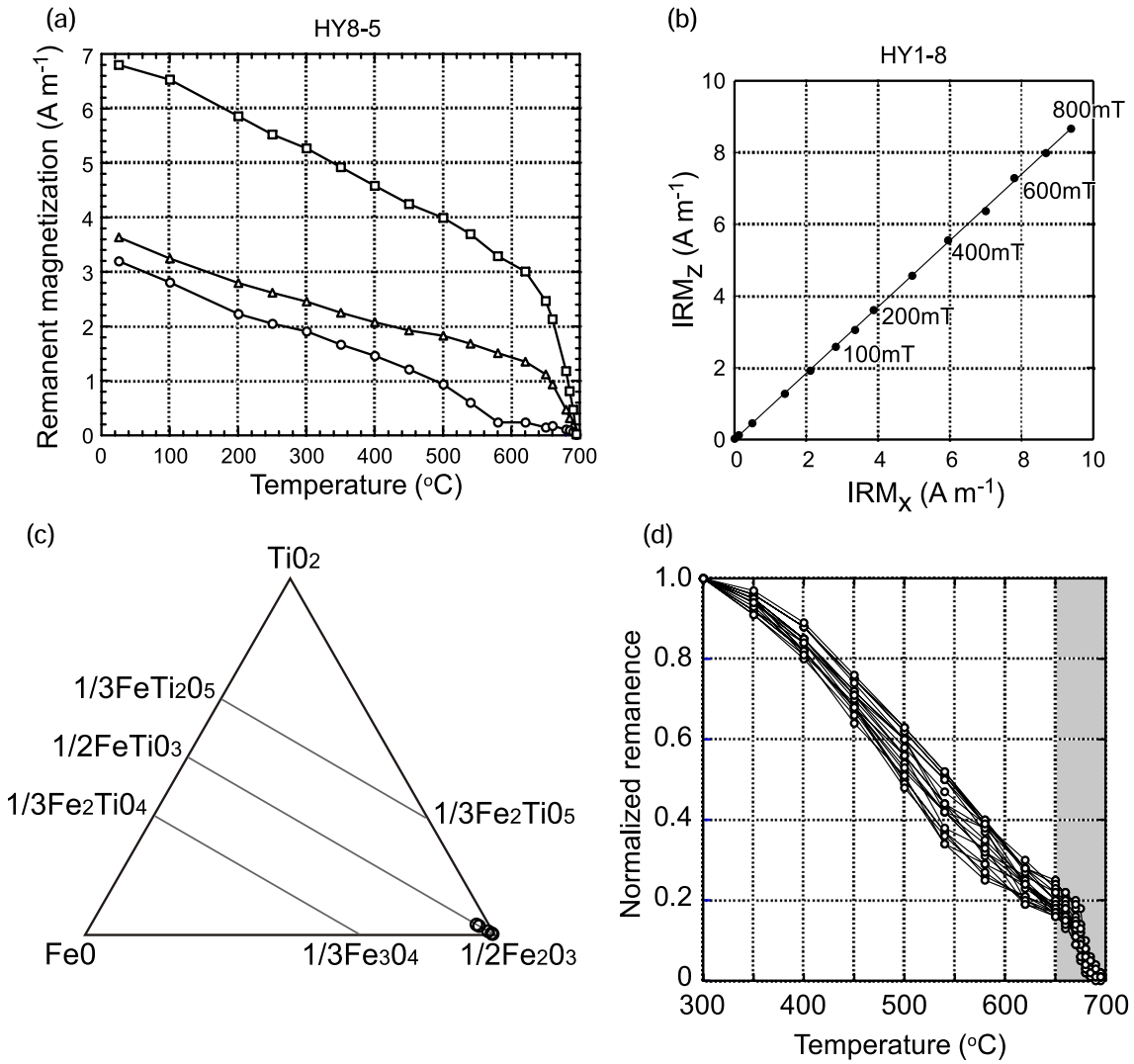

Fig. 4 **a** Thermal demagnetization of the orthogonal three-component IRM: circles indicate the low-coercivity component of the 0.12 T field, triangles indicate the medium-coercivity component of the 0.4 T field, and squares indicate the high-coercivity component of the 2.5 T field. **b** Plot of IRM_Z versus IRM_X showing the gradient of the best-fit correlation line, providing an estimate of the inclination shallowing in sediments. **c** TiO_2–FeO–$1/2Fe_2O_3$ ternary diagram showing chemical compositions of hematite grains in a sample with a laboratory unblocking temperature of 685 °C (HY4-3). Minor components are allocated as follows: $FeO = \Sigma R^{2+} = Fe^{2+} + Mg + Mn$; $Fe_2O_3 = 1/2\Sigma R^{3+} = 1/2(Fe^{3+} + Al)$; $TiO_2 = \Sigma R^{4+} = Ti + Si$. **d** Normalized remanence intensity curves for representative samples. An abrupt decay in intensity is observed in the shaded temperature range (650–695 °C), which is characteristic of DRM (Jiang et al. 2015)

MTC to be a secondary but pre-folding magnetization component. The folding age of the sampled geological unit (Hayama Formation) appears to be before 35.8 Ma because this formation is covered by the 35.8–27.1 Ma Kibi Group with no significant tilting (Suzuki et al. 2003). These results suggest that the age of acquisition of MTCs is constrained to be after 70 Ma and before 35.8 Ma.

The eight directions of HTC had a precision parameter (k value) ranging from 38.0 to 148.9 (Table 1). The mean directions before and after tilt correction were $D = 66.7°$ and $I = 45.8°$ with $\alpha_{95} = 5.2°$ and $D = 65.8°$ and $I = 45.9°$ with $\alpha_{95} = 5.2°$, respectively (Fig. 5c, d). The former mean direction is significantly different from the present Earth's field direction and the geocentric axial dipole field direction in the study area. Since the Hayama Formation formed at approximately 100 Ma, the dominance (100%) of normal polarity for HTC is expected based on the geomagnetic polarity time scale (Cretaceous Normal Superchron, CNS, 121–84 Ma, Ogg 2020), if this component is of primary origin.

There was no difference in the precision parameter of the mean directions before and after tilt correction

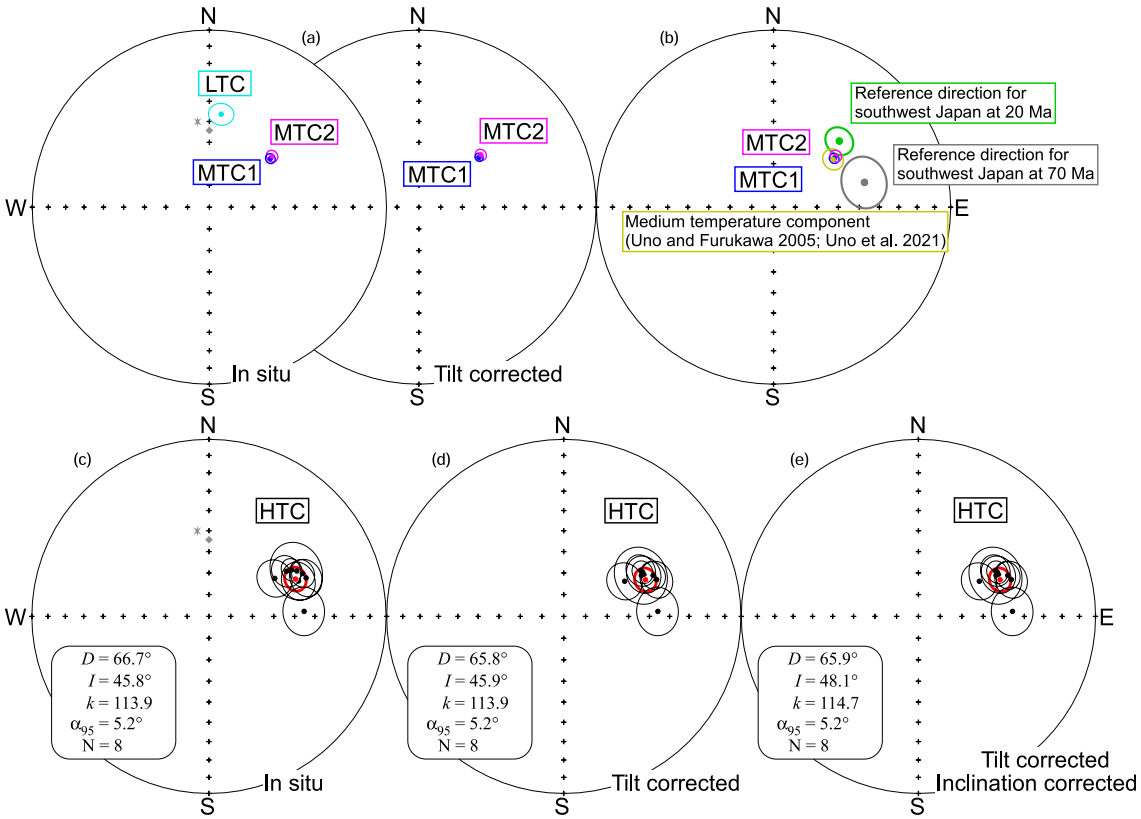

Fig. 5 **a** Equal-area projections of mean directions (with an associated 95% confidence limit) of LTC, MTC1, and MTC2, **b** and those depicted along with the directions of the previously observed medium-temperature component of Cretaceous red beds from southwest Japan (Uno and Furukawa 2005; Uno et al. 2021) and the reference direction for southwest Japan at 70 and 20 Ma (Uno et al. 2021). The asterisk and diamond represent the present Earth's field direction and axial dipole field direction, respectively. **c**–**e** Site-mean directions of HTC. The red symbols represent the mean direction and associated 95% confidence limit

(Fig. 5c, d, Table 1). The fold test of McFadden (1990) yielded an inconclusive test result at the 95% confidence level. As the bedding attitudes at the eight sampling sites had very shallow dipping (flat to 6°), the fold test was not effective in detecting a pre-folding origin for HTC. It should also be noted that α_{95} remained constant at 5.2° after tilt correction.

We calculated the IRM_Z/IRM_X ratio for each site and applied it to tilt-corrected inclination (Fig. 4b, Table 1). The inclination flattening of the sites was up to 2.9°. The mean tilt-corrected direction of the Hayama Formation after inclination correction was $D=65.9°$ and $I=48.1°$, with $\alpha_{95}=5.2°$ ($N=8$) (Fig. 5e). This direction can be regarded as the representative direction of the Hayama area during the mid-Cretaceous (100 Ma).

Observations of polished thin sections under reflected light were conducted to identify the presence of iron oxides in the sampled rock. Subangular to subrounded Fe-Ti grains, up to tens of micrometers in size, were sporadically distributed throughout the sample. These grains as well as other particles such as quartz, feldspar, and lithic fragments, constitute the detrital material (Fig. 6). The Fe-Ti grains revealed a distinctive reflection anisotropy under polarized reflected light, indicating that these grains belong to the ilmenite-hematite solid solution series (Battey 1967).

Chemical composition analysis of the grains was performed using a sample with a laboratory unblocking temperature of 685 °C (HY4-3). They are composed of iron oxides with small quantities of titanium and ionic substitutions by other cations (i.e. nearly pure hematite with minor titanium, Fig. 4c), which predicts a laboratory unblocking temperature of ~ 680 °C. The chemical composition data support a close connection between the observed and expected unblocking temperatures of hematite, suggesting that the detrital hematite grains are correlated with the HTC carrier of the studied red mudstone.

Table 1 Site and formation mean paleomagnetic results of the Hayama Formation

Site	Formation	Lithology	*N(n)*	In situ		Tilt corrected		*I* corrected				Locality		Strike	Dip	IRM_Z/IRM_X
				D(°)	*I*(°)	*D*(°)	*I*(°)	*D*(°)	*I*(°)	*k*	$\propto_{95}$(°)	Lat.(°)	Long.(°)	(°)	(°)	
HY1	Hayama	red ms	7(8)	60.7	45.5	60.7	45.5	60.7	47.7	148.9	5.0	34.817	133.493	0	0	0.924
HY2	Hayama	red ms	7(8)	60.0	54.7	60.0	54.7	60.0	57.4	53.7	8.3	34.817	133.493	0	0	0.903
HY3	Hayama	red ms	7(7)	59.8	48.0	59.3	45.1	59.3	48.0	75.9	7.0	34.817	133.493	320	3	0.902
HY4	Hayama	red ms	5(7)	62.7	43.5	62.2	46.4	62.2	49.0	38.0	12.6	34.817	133.492	162	3	0.914
HY5	Hayama	red ms	7(8)	68.4	40.7	68.4	40.7	68.4	43.0	59.0	7.9	34.817	133.492	0	0	0.922
HY6	Hayama	red ms	8(8)	65.3	41.6	65.3	41.6	65.3	43.8	86.0	6.0	34.817	133.492	0	0	0.923
HY7	Hayama	red ms	3(9)	87.0	45.3	87.0	45.3	87.0	45.8	144.0	10.3	34.818	133.492	0	0	0.983
HY8	Hayama	red ms	4(8)	68.4	44.8	62.4	45.5	62.4	47.7	126.5	8.2	34.787	133.502	239	6	0.927
In situ mean			8*	66.7	45.8					113.9	5.2	34.82	133.49			
Tilt corrected mean						65.8	45.9			113.9	5.2					
Inclination corrected mean								65.9	48.1	114.7	5.2					
Paleomagnetic pole			*N*					Lat.(°)	Long.(°)		A_{95}					
			8*					35.0	209.6		6.1					

Site	*N*	In situ		Tilt corrected		*k*	$\propto_{95}$(°)	Locality	
		D(°)	*I*(°)	*D*(°)	*I*(°)			Lat.(°)	Long.(°)
Low-temperature component									
In situ mean	36	7.3	46.2			20.6	5.4	34.82	133.49
Medium-temperature component 1									
In situ mean	8*	51.5	53.7			618.9	2.2	34.82	133.49
Tilt corrected mean				50.4	53.6	895.0	1.9		
Medium-temperature component 2									
In situ mean	8*	50.9	52.3			434.7	2.7	34.82	133.49
Tilt corrected mean				49.9	52.2	472.0	2.6		

ms mudstone, *N(n)*: number of samples/sites* in calculation for the means (number of samples collected), *D* and *I* declination and inclination, respectively, *k* the precision parameter, $\propto_{95}$ radius of the cone of 95% confidence, *Lat.* north latitude, *Long.* east longitude, A_{95} radius of the circle of 95% confidence

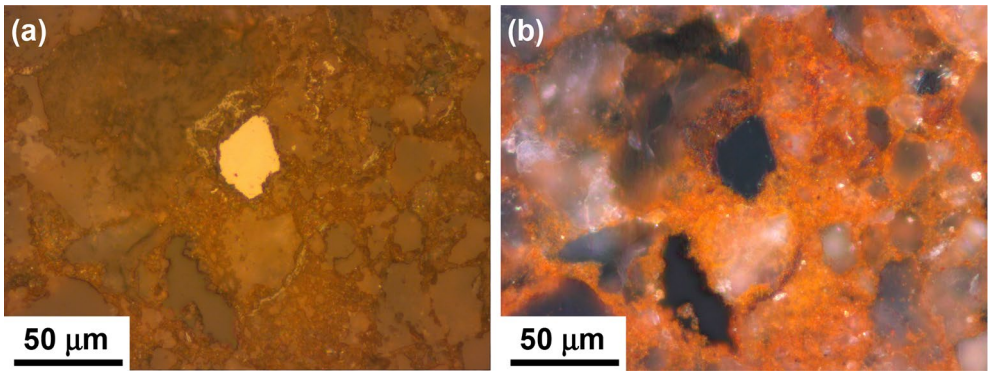

Fig. 6 Photomicrographs of sample HY4-3 in **a** plane and **b** polarized reflected light, showing hematite grain as detrital particles

Discussion

HTC that resides in hematite can be regarded as the primary detrital remanent magnetization (DRM) carried by specular hematite. The remanence carried by specular hematite typically has unblocking temperatures above ~ 650 °C and can be discriminated from the remanence carried by pigmentary hematite, which generally has unblocking temperatures below ~ 650 °C (Jiang et al. 2015). As pigmentary hematite occurs through a chemical process (i.e. hematite pigmentation) after the deposition of strata, it possesses secondary chemical remanent magnetization (CRM). The observed HTC most commonly appeared above ~ 650 °C and was unblocked by 695 °C. Jiang et al. (2015) further argued that based on the shape of remanence intensity curves during thermal demagnetization, DRM carried by specular hematite can be distinguished from CRM carried by pigmentary hematite. DRM decays abruptly at temperatures above 650 °C, whereas CRM gradually decays and is unblocked at ~ 650 °C. We present the normalized intensity curves of the studied samples in Fig. 4d. An abrupt decrease in the intensity is observed in the temperature range of 650–695 °C, indicating a DRM-type shape. Therefore, HTC can be ascribed to the primary magnetization carried by specular hematite, which was ascertained by microscopic observation.

The authors of a previous paleomagnetic study of southwest Japan at ~ 100 Ma (Kodama and Takeda 2002) performed microscopic observations of red beds, and found no presence of specular hematite. Several researchers who have analyzed the remanent magnetization of red beds have emphasized the importance of finding detrital specular hematite in samples by microscopic examination (e.g. Tsuchiyama et al. 2016; Swanson-Hysell et al. 2019). The present study marks the first discovery of detrital specular hematite correlated with the primary magnetization in red beds of ~ 100 Ma in this region, which is of great importance for the construction of reliable APWPs based on reliable datasets.

The angular standard deviation (ASD) may be calculated using the sample- and site-based paleomagnetic poles of HTC of the Hayama Formation, yielding 12.1° and 8.9°, respectively. These values appear to be similar to those expected for a paleolatitude of the study area at the time of deposition (ASD = ~ 8–14° at a paleolatitude of 29.1°, Biggin et al. 2008). The ASD of our data was derived from samples of fine sediments (mudstone) that could potentially contain a long-term geomagnetic field direction in a single specimen. Therefore, our dataset appears to represent the averaged geomagnetic field directions rather than a fairly short-term or spot-reading of the geomagnetic field direction.

A mid-Cretaceous (100 Ma) paleomagnetic pole for the Hayama area in southwest Japan was calculated based on the representative paleomagnetic directions of this area. It is located at 35.0°N and 209.6°E with $A_{95} = 6.1°$ ($N = 8$). The reliability of the pole was assessed using the criteria of Huang et al. (2018), which is a reinterpretation of the Van der Voo (1990) criteria. According to Huang et al. (2018), a paleomagnetic pole that can be incorporated into the pole database for a region needs to yield a quality factor ≥ 4 to meet the following criteria: (1) treatment by progressive demagnetization using principal component analysis (Kirschvink 1980), (2) 24 or more samples yielding a 95% confidence limit (A_{95}) of < 16°, and (3) no suspicion of remagnetization or evidence of significant local rotation. The pole for the Hayama area meets these criteria with a quality factor of 4 and is considered to be a representative candidate for southwest Japan at 100 Ma. This pole corresponds to reliability scores of 4 and 3, using the criteria of Van der Voo (1990) and Meert et al. (2020), respectively.

To obtain a more accurate estimate of the mid-Cretaceous (100 Ma) paleomagnetic pole for southwest Japan, we examined the previously reported 100 Ma pole for

this region. The previously reported 100 Ma pole was led from the San'in and Goshonoura areas (Si and G in Fig. 1a) by Otofuji and Matsuda (1987) and Kodama and Takeda (2002), respectively. A mean pole obtained by averaging the data from the two studies is illustrated in Fig. 1b (187.8°N and 40.6°E with $A_{95}=5.7°$). The pole is located on the near side with respect to other Cretaceous poles in southwest Japan. We assumed that the pole on the near side resulted from the inadequate isolation of a high-temperature component from lower-temperature secondary components and/or insufficient interpretation of the geological structures of the studied rocks. Kodama and Takeda (2002) identified the component C (high-temperature component) that appears at temperatures of 440 °C or higher. However, careful examination of the demagnetization trajectory helped identify a true high-temperature component at temperatures above 580–620 °C. Figure 7 illustrates the magnetization components separated at temperatures between 580 and 620 °C, after which a magnetization component with lower inclination values emerges on the orthogonal vector diagram. This suggests that a component with a shallower inclination should have been derived. On the other hand, Otofuji and Matsuda (1987) identified a high-temperature component using the 100 Ma welded tuff. They adopted a tilt-corrected direction as the primary nature without field tests. We conducted the fold test of McFadden (1990) using their dataset, and an inconclusive test result was obtained at the 95% confidence level ($\xi_1=9.05$ and 14.9 before and after tilt correction, respectively, and a critical value of $\xi_c=5.34$ at the 95% confidence level), but the classical fold test of McElhinny (1964) provided a negative test result at the 95% confidence level ($k_1/k_2=1.81$, $N=21$). It is difficult to identify the paleohorizontal plane in the outcrops of the welded tuff as an eutaxitic structure, defined by stretched pumice lineation, cannot always indicate a paleohorizontal plane (Otofuji et al. 2015). Attempts by Otofuji and Matsuda (1987) to retrieve paleomagnetic directions at 100 Ma using welded tuff may have been unsuccessful.

Consequently, at present, the 100 Ma paleomagnetic pole that is representative of southwest Japan is derived from the data of the Hayama area, the central part of southwest Japan. This area is the most stable continental tectonic unit in southwest Japan (Kibi Plateau, Sonehara et al. 2020) and is suitable for providing a paleomagnetic pole that represents a tectonic domain. The 100 Ma paleomagnetic pole for southwest Japan defined in this study interpolates the Cretaceous APWP for this region as the Cretaceous dataset is composed of 110, 90, 80, and 70 Ma paleomagnetic poles. The 100 Ma pole falls into a cluster of Cretaceous poles in southwest Japan. An

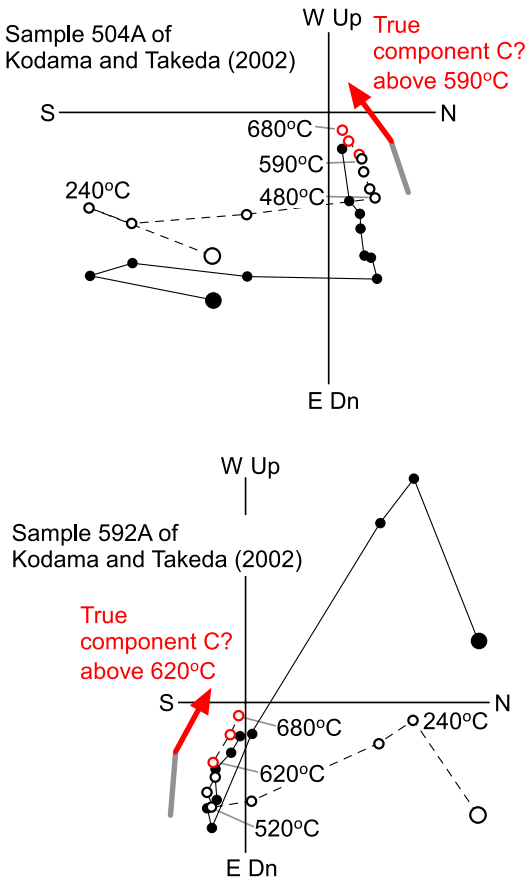

Fig. 7 Analysis of the orthogonal plots of thermal demagnetization results of Kodama and Takeda (2002) showing a true component C (high-temperature component)

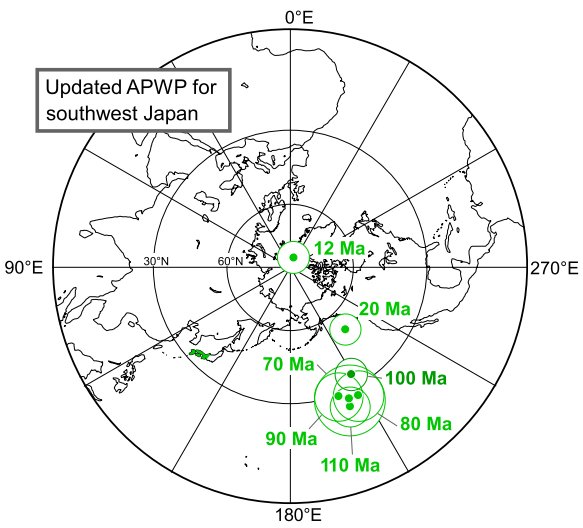

Fig. 8 APWP for southwest Japan from the Early Cretaceous to Miocene (with an associated 95% confidence limit). Pole data after Uno et al. (2021) except for 100 Ma

updated Cretaceous APWP for southwest Japan further confirmed a standstill polar position during 110–70 Ma, as suggested by Uno et al. (2021) (Fig. 8). The quiescence in polar motion during this time interval is consistent with the ~ 130–70 Ma stagnation of pole positions in East Asia as well as Europe (Torsvik et al. 2012; Cogné et al. 2013). Therefore, it is unlikely that the APWP for southwest Japan experienced a hairpin turn during the Cretaceous.

The addition of the newly obtained 100 Ma pole to the APWP data for southwest Japan has helped confirm the absence of the hypothesized Cretaceous tectonic movement. The APWP for southwest Japan has been renewed, and we can summarize the tectonic movements that have affected southwest Japan since 110 Ma. During the Cretaceous, when southwest Japan was attached to East Asia, it behaved as a stable integral part of the continental interior. The tectonics of southwest Japan after the Cretaceous may be described in terms of tectonic rotations without significant latitudinal displacement relative to East Asia. The net rotation degree after the Cretaceous was calculated as the rotation angle with respect to the 70 Ma pole for East Asia, which is located at 79.7°N and 219.5°E with $A_{95} = 3.3°$ (Cogné et al. 2013), leading to a $61.1 \pm 10.6°$ clockwise rotation with $6.4 \pm 9.4°$ insignificant poleward displacement. This large rotation is interpreted as a superimposition of two tectonic rotations of different ages for southwest Japan with respect to East Asia: the earlier rotation is considered to have occurred between 70 and 20 Ma, and the later rotation between 20 and 12 Ma (further constrained by Uno et al. 2021 to be between ~ 17.5 and 14.2 Ma).

Conclusions

As the roundtrip oscillation in the APWP for southwest Japan was assumed to be approximately 100 Ma, which predicts extraordinary latitudinal tectonic translation, we evaluated the paleomagnetic pole for this region during the Cretaceous. The position of the updated 100 Ma pole for southwest Japan was obtained from the remanence carried by detrital specular hematite, and is consistent with the poles of the previous (110 Ma) and subsequent (90–70 Ma) ages. This leads to the conclusion that the APWP for southwest Japan did not include a hairpin turn during the Cretaceous. With the new 100 Ma pole, we updated the APWP for southwest Japan from the Early Cretaceous (110 Ma) onward, showing that the tectonics that affected southwest Japan are essentially described in terms of cumulative clockwise rotation after the Cretaceous with respect to the stable East Asian continent.

Methods

In the laboratory, each oriented hand sample was cored and cut into cylindrical specimens with a diameter of 25 mm and length of 22 mm. Samples from two sites (HY7 and HY8) were friable and challenging to drill to produce a standard-size sample, resulting in some samples being discarded. NRMs were measured using a Natsuhara SMM-85 spinner magnetometer. The samples were subjected to progressive thermal demagnetization using a Natsuhara TDS-1 thermal demagnetizer in a series of 50 °C steps from 200 to 500 °C. The demagnetization steps of 5, 10, 20, 30, and 40 °C were used at temperatures above 580 °C. Results for each sample were plotted on orthogonal vector diagrams (Zijderveld 1967) to interpret magnetic components, as well as on equal-area projections, to evaluate directional stability. After visual inspection of these diagrams and projections, the paleomagnetic directions were determined by principal component analysis based on non-anchored fits (Kirschvink 1980) using at least three demagnetization steps. The maximum angular deviation (MAD) values of the computed linear fits were below 15°. Paleomagnetic data were analyzed using Hatakeyama's (2018) software applications.

Experiments were conducted on the selected samples. Thermal demagnetization of a three-component IRM (Lowrie 1990) was conducted using a magnetic measurement pulse magnetizer (MMPM10) to determine the ferromagnetic mineral content. IRMs of 2.5, 0.4, and 0.12 T were applied sequentially to three orthogonal axes of each sample.

To obtain a high-fidelity record of the Cretaceous magnetic field of the Hayama area, we assessed the inclination shallowing of the remanent magnetization component of the Hayama Formation using the anisotropy of the IRM and correction method of Hodych and Buchan (1994). A representative sample was selected from each site. A magnetic field of up to 800 mT was progressively applied 45° to the bedding plane of the samples to avoid field-impressed anisotropy. IRM was measured at each step parallel (IRM_X) and perpendicular (IRM_Z) to the bedding plane. IRM_Z was plotted against IRM_X, and the IRM_Z/IRM_X ratio was calculated based on the slope of the least-squares fit line for each plot. This ratio can be used to indicate the amount of inclination shallowing using $\tan I_N / \tan I_F = IRM_Z/IRM_X$, where I_N is the inclination of the remanence and I_F is the inclination of the field in which it was acquired.

The polished thin sections of the red mudstone samples were examined using a Carl Zeiss optical microscope to identify the occurrence and texture of iron oxides.

A JEOL JXA8200 electron probe microanalyzer at Kochi University was used to determine the chemical

compositions of the iron oxides. The operating conditions were 12 nA beam current, 15 kV accelerating voltage, and beam diameter of 5 μm. As the total iron content is expressed as FeO, analytical data for the iron oxides were recalculated based on oxide stoichiometry to determine the Fe_2O_3 and FeO contents from the total iron content (Saito et al. 2007).

Abbreviations

APWP	Apparent polar wander path
IGRF	International Geomagnetic Reference Field
NRM	Natural remanent magnetization
LTC	Low-temperature component
MTC	Medium-temperature component
HTC	High-temperature component
IRM	Isothermal remanent magnetization
CNS	Cretaceous Normal Superchron
DRM	Detrital remanent magnetization
CRM	Chemical remanent magnetization
ASD	Angular standard deviation
MAD	Maximum angular deviation

Acknowledgements
We have benefited from discussions with Tadahiro Hatakeyama and Yo-ichiro Otofuji. We are grateful to Xixi Zhao and an anonymous reviewer for valued reviews of the manuscript and suggestions for improvement. The chemical composition analysis was performed under the cooperative research program of the Center for Advanced Marine Core Research, Kochi University (22A018 and 22B017). We thank Yuhji Yamamoto for access to the laboratory.

Author contributions
KU conceptualized the study, conducted fieldwork, analyzed the data, and wrote the manuscript. HO and TK conducted measurements and analyzed the data. KF conceptualized the study, analyzed the data, and wrote the manuscript. All authors read and approved the final manuscript.

Funding
Not applicable.

Availability of data and materials
The datasets used and/or analysed during the current study are available from the corresponding author on reasonable request.

Declarations

Competing interests
The authors declare that they have no competing interests.

Received: 19 June 2022 Accepted: 5 April 2023
Published online: 24 April 2023

References

Battey MH (1967) The identification of the opaque oxide minerals by optical and X-ray methods. In: Collinson DW, Creer KM, Runcorn SK (eds) Methods in paleomagnetism. Elsevier, Amsterdam, pp 485–495
Besse J, Courtillot V (1991) Revised and synthetic apparent polar wander paths of the African, Eurasian, North American and Indian Plates, and true polar wander since 200 Ma. J Geophys Res 96:4029–4050
Besse J, Courtillot V (2002) Apparent and true polar wander and the geometry of the geomagnetic field over the last 200 Myr. J Geophys Res 107:2300. https://doi.org/10.1029/2000JB000050
Biggin AJ, van Hinsbergen DJJ, Langereis CG, Straathof GB, Deenen MHL (2008) Geomagnetic secular variation in the Cretaceous Normal Superchron and in the Jurassic. Phys Earth Planet Inter 169:3–19
Cogné JP, Besse J, Chen Y, Hankard F (2013) A new Late Cretaceous to Present APWP for Asia and its implications for paleomagnetic shallow inclinations in Central Asia and Cenozoic Eurasian plate deformation. Geophys J Int 192:1000–1024
Gordon RG, Cox A, O'Hare S (1984) Paleomagnetic Euler poles and the apparent polar wander and absolute motion of North America since the Carboniferous. Tectonics 3:499–537
Hatakeyama T (2018) Online plotting applications for paleomagnetic and rock magnetic data. Earth Planets Space 70:139
Hodych JP, Buchan KL (1994) Early Silurian palaeolatitude of the Springdale Group redbeds of central Newfoundland: a palaeomagnetic determination with a remanence anisotropy test for inclination error. Geophys J Int 117:640–652
Huang B, Yan Y, Piper JDA, Zhang D, Yi Z, Yu S, Zhou T (2018) Paleomagnetic constraints on the paleogeography of the East Asian blocks during Late Paleozoic and Early Mesozoic times. Earth Sci Rev 186:8–36
Jiang Z, Liu Q, Dekkers MJ, Tauxe L, Qin H, Barrón V, Torrent J (2015) Acquisition of chemical remanent magnetization during experimental ferrihydrite–hematite conversion in Earth-like magnetic field—implications for paleomagnetic studies of red beds. Earth Planet Sci Lett 428:1–10
Jolivet L, Tamaki K, Fournier M (1994) Japan Sea, opening history and mechanism: A synthesis. J Geophys Res 99:22237–22259
Kirschvink JL (1980) The least-square line and plane and the analysis of palaeomagnetic data. Geophys J Roy Astron Soc 62:699–718
Kodama K, Takeda T (2002) Paleomagnetism of mid-Cretaceous red beds in west-central Kyushu Island, southwest Japan: paleoposition of Cretaceous sedimentary basins along the eastern margin of Asia. Earth Planet Sci Lett 201:233–246
Lee YI (2008) Paleogeographic reconstructions of the East Asia continental margin during the middle to late Mesozoic. Island Arc 17:458–470
Lowrie W (1990) Identification of ferromagnetic minerals in a rock by coercivity and unblocking temperature properties. Geophys Res Lett 17:159–162
McElhinny MW (1964) Statistical significance of the fold test in palaeomagnetism. Geophys J Roy Astron Soc 135:338–340
McFadden PL (1990) A new fold test for palaeomagnetic studies. Geophys J Int 103:163–169
Meert JG, Pivarunas AF, Evans DAT, Pisarevsky SA, Pesonen LJ, Li ZX, Elming SÅ, Miller SR, Zhang S, Salminen JM (2020) The magnificent seven: A proposal for modest revision of the Van der Voo (1990) quality index. Tectonophysics 790:228549
Ogg JG (2020) Geomagnetic polarity time scale. In: Gradstein FM, Ogg JG, Schmitz MD, Ogg GM (eds) A geologic time scale 2020. Elsevier, Amsterdam, pp 159–192
Otofuji Y, Matsuda T (1987) Amount of clockwise rotation of Southwest Japan—fan shape opening of the southwestern part of the Japan Sea. Earth Planet Sci Lett 85:289–301
Otofuji Y, Matsuda T, Nohda S (1985) Opening mode of the Japan Sea inferred from the palaeomagnetism of the Japan Arc. Nature 317:603–604
Otofuji Y, Zaman H, Shogaki G, Seki H, Polin VF, Miura D, Ahn HS, Ivanov Yu, Minyuk P, Zimin P (2015) Paleomagnetism of the Late Cretaceous ignimbrite from the Okhotsk-Chukotka Volcanic Belt, Kolyma-Omolon Composite Terrane:Tectonic implications. J Geodyn 91:1–12
Saito T, Ishikawa N, Kamata H (2007) Magnetic petrology of the 1991–1995 dacite lava of Unzen volcano, Japan: Degree of oxidation and implications for the growth of lava domes. J Volcanol Geoth Res 164:268–283
Seguin MK, Zhai Y (1992) Paleomagnetic constraints on the crustal evolution of the Yangtze block, southeastern China. Tectonophysics 210:59–76
Sonehara T, Yagi K, Takeshita H, Aoki K, Aoki S, Otofuji Y, Itaya T (2020) Kibi Plateau: A stable-coherent tectonic unit in the active Japanese Islands. Sci Rep 10:3786. https://doi.org/10.1038/s41598-020-60448-x
Suzuki S, Asiedu DK, Fujiwara T (2001) Lower Cretaceous fluvial deposits, Hayama Formation, Nariwa Area, Okayama Prefecture, Southwest Japan. J Geol Soc Jpn 107:541–556
Suzuki S, Danhara T, Tanaka H (2003) Fission-track dating of Tertiary tuff samples from the Kibi Plateau area, Okayama Prefecture, Southwest Japan. J Geogr 112:35–49

Swanson-Hysell NL, Fairchild LM, Slotznick SP (2019) Primary and secondary red bed magnetization constrained by fluvial intraclasts. J Geophys Res 124:4276–4289
Torsvik TH, Van der Voo R, Preeden U, Mac Niocaill C, Steinberger B, Doubrovine PV, van Hinsbergen DJJ, Domeier M, Gaina C, Tohver E, Meert JG, McCausland PJA, Cocks LRM (2012) Phanerozoic polar wander, palaeogeography and dynamics. Earth Sci Rev 114:325–368
Tsuchiyama Y, Zaman H, Sotham S, Samuth Y, Sato E, Ahn HS, Uno K, Tsumura K, Miki M, Otofuji Y (2016) Paleomagnetism of Late Jurassic to Early Cretaceous red beds from the Cardamom Mountains, southwestern Cambodia: Tectonic deformation of the Indochina Peninsula. Earth Planet Sci Lett 434:274–288
Uno K, Furukawa K (2005) Timing of remanent magnetization acquisition in red beds: a case study from a syn-folding sedimentary basin. Tectonophysics 406:67–80
Uno K, Furukawa K, Hatanaka Y (2017) An analysis of apparent polar wander path for southwest Japan suggests no relative movement with respect to Eurasia during the Cretaceous. Phys Earth Planet Inter 267:19–30
Uno K, Idehara Y, Morita D, Furukawa K (2021) An improved apparent polar wander path for southwest Japan: post-Cretaceous multiphase rotations with respect to the Asian continent. Earth Planets Space 73:132
Van der Voo R (1990) The reliability of paleomagnetic data. Tectonophysics 184:1–9
Westphal M, Bazhenov M, Lauer JP, Pechersky D, Sibuet J (1986) Paleomagnetic implications on the evolution of the Tethys belt from the Atlantic Ocean to the Pamirs since the Triassic. Tectonophysics 123:37–82
Zijderveld JDA (1967) A.C. demagnetization of rocks: analysis of results. In: Collinson DW, Creer KM, Runcorn SK (eds) Methods in paleomagnetism. Elsevier, Amsterdam, pp 254–286

Publisher's Note